A real support effect on the hydrodeoxygenation of methyl oleate by sulfided NiMo catalysts

Document Version:
Publisher's PDF, also known as Version of Record (includes final page, issue and volume numbers)

Please check the document version of this publication:

• A submitted manuscript is the version of the article upon submission and before peer-review. There can be important differences between the submitted version and the official published version of record. People interested in the research are advised to contact the author for the final version of the publication, or visit the DOI to the publisher's website.
• The final author version and the galley proof are versions of the publication after peer review.
• The final published version features the final layout of the paper including the volume, issue and page numbers.

Link to publication

Download date: 04. Oct. 2023

A real support effect on the hydrodeoxygenation of methyl oleate by sulfided NiMo catalysts

CrossMark

A.E. Coumans, E.J.M. Hensen*

Laboratory of Inorganic Materials Chemistry, Schuit Institute of Catalysis, Eindhoven University of Technology, P.O. Box 513, 5600 MB Eindhoven, The Netherlands

ABSTRACT

The effect of the support on the catalytic performance of sulfided NiMo in the hydrodeoxygenation of methyl oleate as a model compound for triglyceride upgrading to green diesel was investigated. NiMo sulfides were prepared by impregnation and sulfidation on activated carbon, silica, γ-alumina and amorphous silica-alumina (ASA). High sulfidation degrees were obtained in all cases. Despite the use of a chelating agent to minimize metal-support interactions, the support had a significant influence on the morphology of the active phase (MoS_2 dispersion and stacking). All catalysts convert methyl oleate to C17 and C18 olefins and paraffins. Initially, NiMo/Al_2O_3 and NiMo/ASA displayed the highest overall HDO activity, but these catalysts deactivated slowly during the week on stream. Finally, they exhibited similar activity as NiMo/SiO_2. NiMo/C and NiMo/SiO_2 did not deactivate. The NiMo/C catalyst was appreciably more active than the others after prolonged reaction. The high initial and then deactivating performance of NiMo/Al_2O_3 and NiMo/ASA is due to the Lewis acidity of surface Al species active in methyl oleate hydrolysis. It has earlier been demonstrated that deposition of heavy products on the alumina surface deactivates these sites. SiO_2 lacks such sites, resulting in lower catalytic performance. The NiMo/C support is more active in methyl oleate hydrolysis. This can be either due to intrinsically higher activity of the metal sulfide on carbon or to acidic surface groups. Besides, the reaction data show that the C18 hydrocarbons selectivity for NiMo/SiO_2 and NiMo/C was substantially higher than for the other two catalysts. Clearly, the support has a significant influence on the performance of NiMo sulfide in methyl oleate HDO. The use of activated carbon as the support presents high and stable HDO activity of methyl oleate with good C18 hydrocarbons selectivity.

1. Introduction

Environmental concerns about global warming and the finite nature of fossil reserves are the main drivers for the search of alternative renewable liquid fuels. While the overall energy mix continues to diversify, biofuels will remain the main option for aviation, long-distance road transport, and rail where it cannot be electrified [1]. The global context for biofuels is changing little as a result of the recent oil price collapse, as biofuel consumption remains largely mandate-driven and will rise accordingly [2]. Such mandates often relate to political choices, for instance by the European Union to build a biobased economy in which biofuels play a central role [3].

First-generation biofuels are manufactured from edible biomass such as starch-rich or oily plants. Important examples are bio-ethanol obtained by fermentation of sugars and diesel obtained by upgrading of triglycerides. On the other hand, second- and third-generation biofuels derive from non-edible biomass such as woody biomass and waste streams and algae. Whilst more sustainable, the associated conversion

technologies are typically less mature than first-generation biofuels manufacture [4] and involve biochemical and thermochemical processes such as pyrolysis, gasification, supercritical fluid extraction, and direct liquefaction [5,6].

Vegetable oils and animal fats are first-generation biomass feedstock, comprised of triglycerides that can be converted to diesel. Two important routes have been developed to convert triglycerides into transportation fuels. Biodiesel consists of fatty acid methyl esters (FAMEs) obtained by base- or acid-catalyzed transesterification of vegetable oils with alcohols. These reactions do not involve deoxygenation of the feedstock. FAMEs are unstable on storage and may also cause problems when used in combustion engines. This limits the amount of biodiesel that can be blended in diesel fuel [4,7]. Another drawback is that transesterification leads to the co-production of significant amounts of glycerol as low-value byproduct [4]. An alternative approach involves the direct hydrodeoxygenation (HDO) of triglycerides into hydrocarbons. Usually, diesel resulting from HDO is called green diesel or renewable diesel to distinguish it from "biodiesel". The

most common approach is hydrodeoxygenation (HDO) of triglycerides into hydrocarbons in a process akin to the removal of sulfur and nitrogen from petroleum-derived feedstock. These hydrotreating processes typically use metal sulfide catalysts, which require co-feeding H_2S to retain their active sulfided state when sulfur-free biogenic feedstock is upgraded [7,8]. A third approach avoids the use of hydrogen and uses precious metals such as Pt and Pd to remove oxygen from triglycerides [9,10]. Compared with biodiesel, green diesel is compatible with existing combustion engines and has better fuel properties because of its higher cetane number, higher energy density and very low sulfur content [4,7]. It is also possible to obtain lighter hydrocarbons for the jet or gasoline fuel pool by using catalysts with strong acid sites.

Upgrading of this feedstock can either be done by hydroprocessing of triglycerides, or by co-feeding them in petroleum-derived vacuum gas oil upgrading processes. The latter has been explored to limited degree [11,12], while the former appears to be the preferred option in practice. For instance, the UOP/ENI Ecofining process involves hydrotreating followed by isomerization [13]. Neste Oil operates chemical plants in The Netherlands and Singapore that convert palm oil and waste animal fat into green diesel by hydrotreating [14]. The resulting fuel is not a substitute for fossil fuels, rather it is blended with fossil-derived transportation fuels to boost their properties. The catalyst determines the yield and product distribution during triglycerides conversion to a significant extent. Many types of catalysts have been explored for direct hydrotreating of triglycerides, and they are usually comprised of conventional hydrotreating catalysts or zeolites used in petroleum refining. Zeolites in combination with metal sulfide or noble metal hydrogenation functions facilitate hydrocracking, which is preferred when a boiling point shift to gasoline-range hydrocarbons is targeted [11]. Hydroprocessing of triglycerides with NiMo sulfide catalysts yields green diesel [15,16]. A comparative study of Sotelo-Boyas et al. demonstrated the preference of NiMo/γ-Al$_2$O$_3$ over Pt/zeolite systems for obtaining diesel-range hydrocarbons [17].

HDO of triglycerides is preferably done with metal sulfide catalysts, which are also widely employed in the hydrodesulfurization (HDS) of oil fractions in petroleum refineries [18]. Alumina-supported NiMo (and CoMo) sulfide catalysts have already been extensively studied in the context of hydrotreating of petroleum fractions. Several excellent reviews are available [18–22]. These catalysts consist of Co- and Ni-promoted MoS$_2$ supported on γ-alumina. HDO of vegetable oil feedstock using supported NiMo sulfides has been studied in the past [4,9,23,8,24–32]. Usually, model compounds have been employed in this context [25–28,33,34]. Recently, we have investigated the kinetics of the HDO of methyl oleate over a γ-alumina-supported NiMo sulfide catalyst. The support plays a crucial role in the performance of NiMo and CoMo sulfide HDS catalysts [18]. A real support effect on the performance of CoMo sulfide catalysts has been reported for the HDS of thiophene by Van Veen et al. [35]. In hydrotreating operations, γ-alumina is the preferred support to disperse the active Co(Ni)-Mo-S phase. The most active catalysts are obtained when the metals on the support are fully sulfided. On the other hand, some interaction between Mo and the support is usually assumed to be beneficial for high MoS$_2$ dispersion [18]. This is important because the edge surface area, where the active Co (Ni) promoter sites are located, increases with decreasing (lateral) size of the MoS$_2$ slab. The most active phase is referred to as type II, which distinguishes itself from the type I phase by minimized support interaction and high sulfidation degree. Type I NiMoS structures are proposed to be incompletely sulfided in the sense that some Mo-O-Al linkages with the alumina support remain [35,36]. Thus, weak metal-support interaction favors formation of type II structures [35]. This understanding has led to the exploration of other supports for dispersing the active metal sulfide phase. For instance, the support substantially influences the performance in dibenzothiophene HDS and toluene hydrogenation for NiMo and NiW sulfides [37]. It has also been argued that the outstanding performance of CoMo and NiMo sulfides on

activated carbon in HDS model reactions is due to the weak interaction of carbon with the metal sulfides, resulting in type II character of the active phase [35,38]. The low density of activated carbon and deactivation in real feed gas oil tests, presumably due to adsorption of multi-ring aromatics, limit their use in practice [39]. With respect to HDO of vegetable oil feedstock and related model compounds, carbon appears to be promising for dispersing Ni, Pd, and Pt nanoparticles [40–42]. A significant advantage of activated carbon is its high surface area, although it must be noted that a large fraction of the surface area derives from the presence of very small micropores, which may lead to mass transport limitations. Amorphous silica-alumina (ASA), on the other hand, is widely used as a solid acid catalyst in various industrial processes, often in combination with a hydrogenation function provided by Pt(Pd) or Ni(Co)Mo(W) sulfides. In the context of HDO of triglycerides, concerns arise because the acidity may lead to coke formation and unwanted hydrocracking of the feedstock when diesel is the target [43]. On the other hand, acid-catalyzed dehydration reactions may facilitate the HDO of methyl esters [7].

In a recent work, we investigated the kinetics and mechanism of the HDO of methyl oleate, oleic acid and glyceryl trioleate using an alumina-supported NiMo sulfide catalyst under trickle-flow conditions [44]. The alumina-supported NiMo sulfide was found to slowly deactivate during methyl oleate HDO. The hydrogenation activity decreased more pronouncedly with time on stream than the deoxygenation activity and significant build-up of carbonaceous species on the catalyst surface was observed. It was argued that the decreased hydrogenation activity might be linked to stacking of the MoS$_2$ phase, while the loss of hydrolysis activity is due to blocking of Lewis acid sites of the support. Given the importance of a support effect in HDS [35], we expand these earlier investigations by studying the influence of the support on the performance of NiMo sulfide in the HDO of methyl oleate. We prepared NiMo sulfides on γ-Al$_2$O$_3$, SiO$_2$, SiO$_2$-Al$_2$O$_3$ and activated carbon. The acidic properties of these supports will be briefly discussed by reviewing relevant literature. We determined the sulfidation degree, morphology and dispersion of the active phase upon sulfidation and the catalytic performance in the HDS of thiophene HDS and the HDO of methyl oleate.

2. Experimental methods

2.1. Materials

Methyl oleate (ABCR) was used as received. Gas chromatography analysis showed that three isomers of octadecenoic methyl ester made up 86 wt% of the feedstock. About 4 wt% C18 methyl esters with two unsaturated C−C bonds (methyl linoleate) and three unsaturated C−C bonds (methyl linoleneate) were observed. In total, six isomers of these compounds were detected. The remainder of the methyl oleate feed was 10 wt% of methyl palmitate, which is a C16 methyl ester.

2.2. Catalyst preparation

A set of supported NiMo-NTA (NTA = nitrilotriacetic acid) catalysts was prepared by pore volume impregnation. For impregnation, the water pore volume of the supports was determined in triplo. The ASA support was prepared by homogeneous deposition-precipitation of Al^{3+} on silica (∼5 wt% Al$_2$O$_3$ on SiO$_2$) followed by calcination [45]. γ-alumina (Ketjen CK-300), silica (Shell) and activated carbon (NORIT RX-3 extra) were used as received. The acidic properties of the used ASA, SiO$_2$ and Al$_2$O$_3$ have been reported elsewhere [46]. The textural properties of all support materials are collected in Table 1. Prior to impregnation, a sieved fraction of these materials (125–250 μm) was dried overnight at 110 °C. For NiMo-NTA catalysts, the impregnation solution contained the chelating agent nitrilotriacetic acid (VWR, 99% purity), ammonium heptamolybdate (Merck, 99% purity) and nickel nitrate (VWR, 99% purity) in concentrations to obtain a final Mo

Table 1
Properties of the used supports and the prepared catalysts.

Support						Catalyst		
Type	Supplier	S.A. (m^2/g)[a]	P.V. (ml/g)[b]	Acidity (µmol/g)		Sample	Mo loading (wt%)[c]	Ni/Mo (−)[e]
				BAS[c]	LAS[d]			
Carbon	Norit RX3-Extra	1190	1.00	0.2	n.d.	NiMo/C	6.70	0.31
SiO$_2$	Shell	260	1.25	0	0	NiMo/SiO$_2$	6.26	0.30
ASA	Home-made	289	1.75	3.6	59	NiMo/ASA	5.29	0.30
Al$_2$O$_3$	Ketjen CK300	183	0.66	0	340	NiMo/Al$_2$O$_3$	6.45	0.29

[a] BET surface area.
[b] Water pore volume determined after drying at 110 °C overnight.
[c] Brønsted acid sites determined by isopropylamine TPD; data for SiO$_2$, Al$_2$O$_3$ and ASA taken from Ref. [46]; data for Carbon recorded by the procedure outlined in Ref. [46].
[d] Lewis acid sites determined by CO IR [46].
[e] Elemental composition determined by ICP-OES.

loading of 8 wt% and an atomic Ni/Mo ratio of 0.3. The molar NTA to Mo ratio was 1.2 [35]. The catalysts were dried at room temperature for 1 h, dried overnight at 110 °C. They were grinded and sieved to obtain particles with sizes between 125 µm and 250 µm. The Mo loading and the Ni/Mo atomic ratio of were determined by ICP-OES elemental analysis (Spectro CIROS CCD spectrometer, samples dissolved in 1/1/1 vol mixture of HF/HNO$_3$/H$_2$O).

2.3. Catalyst characterization

The porosity of the used supports was determined by N$_2$ physisorption using a Micromeritics Tristar 3000. Typically, 25 mg of sample was first outgassed at 400 °C for 3 h prior to measurement. The Brunauer-Emmett-Teller (BET) equation was used to calculate the specific surface area from the adsorption data obtained.

In order to characterize freshly sulfided catalysts, the catalyst was sulfided in the same manner as for the catalytic activity measurements (*vide infra*) without the pre-bed and the SiC diluent, so that the sulfided catalyst could be retrieved in a form amenable to further surface analyses. The catalysts were removed from the reactors inside a nitrogen-flushed glove box. The samples were stored in the glove box before further characterization.

For X-ray Photoelectron Spectroscopy (XPS) analysis, a specially designed transfer holder was used to take the well-crushed sample from the nitrogen-filled glove box to the XPS apparatus without exposure to air. The XPS measurements were carried out on a Thermo Scientific K-Alpha, equipped with a monochromatic small-spot X-ray source and a 180° double focusing hemispherical analyser with a 128-channel detector. Spectra were obtained using an aluminium anode (Al Kα = 1486.6 eV) operating at 72 W and a spot size of 400 µm. Survey scans were measured at a constant pass energy of 200 eV and region scans at 50 eV. The background pressure was 2×10^{-9} mbar. During measurement, this was 3×10^{-7} mbar Ar because of the charge compensation dual beam source. Energy correction was performed by using the C 1 s peak of adventitious carbon at 284.8 eV as a reference. The resulting spectra were fitted using CasaXPS.

Accurate determination of the dispersion and stacking degree requires that the spent catalysts is transferred from the reactor to the electron microscope without exposure to air [47]. For this purpose, glass ampules were used to transfer the catalysts to the TEM (transition electron microscopy) laboratory at Delft University of Technology. The ampules were then loaded in an Ar-filled glove box and opened. The sample was crushed in *n*-hexane using a mortar to obtain a suspension,

which was then dropped on a Cu holey carbon TEM grid (Quantifoil). The solvent was slowly evaporated at room temperature, after which the TEM grid was placed in a specially designed vacuum transfer TEM holder. The TEM grid was then transported to the TEM avoiding contact to air. TEM measurements were carried out using an FEI Tecnai F20ST/STEM, operated at an accelerating voltage of 200 keV. Images were obtained using a Gatan Ultrascan CCD camera (4k × 4k) in bright-field mode, at a magnification of 440 k×. Per sample, about 50 micrographs were taken. Detailed analysis of these micrographs was carried out by measuring the length and stacking degree using the ImageJ software. In this way, between 500 and 1200 particles were analyzed per sample.

2.4. Catalytic activity measurements

Atmospheric pressure gas-phase thiophene hydrodesulfurization (HDS) was carried out in a single-pass stainless steel micro flow reactor. Gaseous thiophene was obtained by passing hydrogen (99.95%, Hoekloos) through thiophene (Merck, ≥99% purity) maintained in a saturator at a constant temperature of 20 °C. The required thiophene concentration was obtained by diluting this flow with pure hydrogen. Thermal mass flow controllers were used to feed the gaseous flows. The experiments were carried out under differential conditions by diluting an amount of catalyst (sieve fraction 125–250 µm) with SiC of the same sieve fraction. Prior to reaction, the catalysts were sulfided in a mixture of H$_2$S/H$_2$ gas (10 vol% H$_2$S in H$_2$) at a total flow rate of 60 ml/min at atmospheric pressure. The samples were heated at a ramp rate of 2 °C/min. The temperature was kept at 400 °C for 2 h. After sulfidation, the catalyst was exposed to a mixture of 4 vol% thiophene and 1 vol% H$_2$S at this temperature. The total flow rate was maintained at 100 ml/min (STP). After the thiophene conversion was stabilized after 13 h, the temperature was lowered to 350 °C and kinetic measurements were started. Intrinsic reaction rate constants were calculated from the thiophene HDS conversion and corrected for molybdenum edge dispersion as determined *via* HR-TEM (*vide infra*). Hydrocarbon reactants and products was analyzed on a Restek RTX-1 column placed in an Thermo Scientific Trace 1300 GC equipped with a flame ionization detector.

Catalytic hydrodeoxygenation (HDO) activity experiments were carried out in a fixed-bed Hastelloy reactor, which was heated in a three-zone oven. Thermal mass flow controllers were used for the supply of H$_2$, H$_2$S and CO gases. The liquid feed was supplied by a Shimadzu LC-20AD pump. All tubing was heated after the point of introduction of the liquid feed into the gas stream to avoid condensation of reactants and products. The catalyst bed consisted of 0.1 g catalyst mixed with 2.5 g SiC. Before the catalyst bed, a pre-bed was placed consisting of 5 g SiC in order to establish trickle-flow conditions [48]. Prior to reaction, the catalysts were sulfided in a mixture of H$_2$S/H$_2$ gas (10 vol% H$_2$S in H$_2$) at a total flow rate of 60 ml/min at a pressure of 15 bar. The samples were heated at a ramp rate of 2 °C/min. The temperature was kept at 400 °C for 2 h. Then, the temperature of the catalyst bed was lowered to 260 °C and the total pressure was increased to 30 bar. The packed bed was then wetted by maintaining a liquid flow rate of 1 ml/min for 15 min. The reaction was started by adding the gases to the feed. The feed consisted of a mixture of 20 wt% methyl oleate in 1,2,3,4-tetrahydronaphthalene (tetralin, ≥98%, Merck). The weight hourly space velocity (WHSV) during methyl oleate HDO measurements was 6.5 h^{-1}. The gas-to-oil ratio (GOR) was 10,320 Nl kg^{-1} h^{-1} with the gas being composed of H$_2$ containing 2000 ppm H$_2$S.

The liquid phase of the reactor effluent was analyzed on a Restek MXT-Biodiesel TG column (L = 10 m, d$_i$ = 0.32 mm, d$_f$ = 10 µm) placed in an Interscience FocusGC gas chromatograph equipped with a flame ionization detector. Injection was done by a ROLSI system from a small reservoir placed directly after the reactor outlet.

The HDO conversion was determined based on all reaction products in which oxygen was completely removed:

$$X_{HDO} = \frac{n_{C17} + n_{18}}{n_{C17} + n_{18} + n_{oxy}} \times 100\% \qquad (1)$$

Therefore, X_{HDO} involves all deoxygenated products (n_{C17} and n_{C18}) and n_{oxy} groups all oxygenated hydrocarbons. Assuming plug flow conditions over the fixed bed and considering the order for the feedstock to be one, as was found previously [44], the first order rate constant can be calculated from the conversion based on the amount of catalyst (W) and the molar reactant flow (F^O) [49]:

$$k_{HDO} = \frac{-\ln(1 - X_{HDO})F^0}{W} \qquad (2)$$

By using the metal loading and the Mo-edge dispersion derived from HR-TEM analysis (*vide infra*) in the manner described by Kasztelan et al. [50], dispersion-corrected rate constants were calculated. We considered the selectivity of specific oxygenated products among all oxygenated compounds including the feedstock, and further distinguished the C17 and C18 selectivity in which olefins and paraffins were grouped:

$$S_{C17} = \frac{n_{C17}}{n_{C17} + n_{C18}} \times 100\% \qquad (3)$$

We also determined the fraction of olefins for both the C17 and the C18 fractions.

3. Results and discussion

Table 1 contains the basic information about the catalysts used in the present study. The activated carbon, an extensively acid-washed material, has a much higher surface area than the oxide supports. The amorphous silica-alumina sample was prepared by homogeneous deposition-precipitation of Al^{3+} on silica followed by calcination at 800 °C [37].

^{27}Al MAS-NMR spectra of the calcined ASA support and γ-alumina are shown in Fig. 1 and emphasize the difference in Al coordination between the two samples. The sample with a nominal Al content of 5 wt % contains predominantly tetrahedral Al. The amorphous silica-alumina support contains mainly isolated Lewis acid Al^{3+} sites grafted to the silica surface. This is also reflected in the higher symmetry of the Al^{IV} contribution in the ASA, as compared to the disordered nature of the NMR peaks of γ-Al_2O_3 [51]. Earlier characterization has shown that calcination of the grafted Al species on the silica surface leads to diffusion of a very small fraction of Al into the silica network and generation of few Brønsted acid sites [45,52]. The single pulse ^{27}Al NMR spectra were deconvoluted into Al^{IV} and Al^{VI} contributions (Fig. 1).
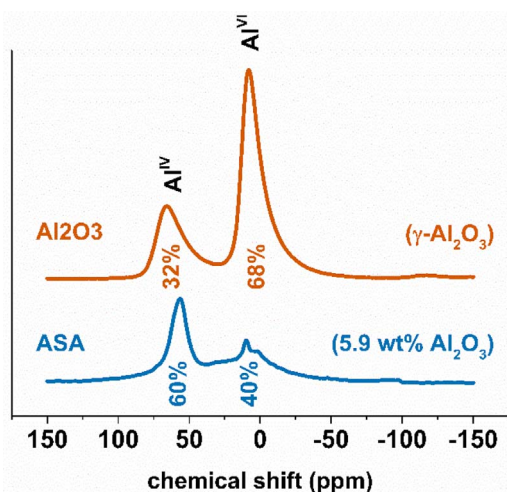

Fig. 1. ^{27}Al MAS NMR spectra of the ASA and γ-alumina supports, showing the contributions of Al^{IV} (56–66 ppm) and Al^{VI} (9 ppm) species as determined by deconvolution. The aluminium content of the ASA sample was determined by ICP-OES.

The acidic properties of these support materials, mostly taken from literature [46], are collected in Table 1. The number of strong Brønsted acid sites (BAS) in these samples were obtained by decomposition of adsorbed isopropylamine, the number of Lewis acid sites by infrared spectroscopy of adsorbed CO at 80 K. The number of BAS on silica and γ-alumina is negligible. The silica-alumina material contains about 3.6 µmol/g, a much smaller number than present in crystalline aluminosilicate zeolites [46]. The activated carbon support contains only a very small amount of strong BAS. While the γ-alumina support contains a large number of mainly weak Lewis acid sites, the amorphous silica-alumina support contains much less LAS, most of them being strong LAS [46]. As expected, the silica support does not contain LAS. The number of LAS in the activated carbon support could not be determined by infrared spectroscopy. We expect this number to be very low, because the used support has been extensively washed with nitric acid to remove metal contaminants. Although preferably one would like to relate catalytic performance data to the acidity of the actual catalysts, probing acidity by most established methods is not selective for the support and the active metal sulfide phase would certainly make interpretation of these data cumbersome, if not impossible. Therefore, a basic assumption is that the acidity in the final sulfided catalysts correlates to the acidity of the parent supports.

Using activated carbon, silica, γ-alumina and silica-alumina as carrier materials, catalysts were prepared by pore volume impregnation with a solution containing suitable metal precursors and NTA. The Ni/Mo ratios in the catalysts were close to the optimal value of 0.30 [53]. The use of NTA as a chelating agent served the goal of minimizing metal support interactions in order to end up with similar NiMo sulfide phases after sulfidation [35]. We characterized the sulfided catalysts by HR-TEM, XPS, and thiophene HDS. To determine the dispersion and morphology of the active phase, high resolution transition electron microscopy (HR-TEM) was done. Representative transmission electron micrographs of sulfided $NiMo/SiO_2$ and $NiMo/Al_2O_3$ can be seen in Fig. 2.

The images show the MoS_2 slabs by their edge planes oriented in line with or slightly tilted from the electron beam. The slabs are present as single slabs as well as in stacks. Fig. 2 also depicts the slab size distribution for these two samples. Parameters describing the MoS_2 phase in terms of average particle size and stacking degree were derived from accurate analysis of 500–1200 slabs per sample. The resulting data are summarized in Table 2.

The average length of the MoS_2 slabs is around 2–3 nm, in good agreement with reported data [54]. Sulfided $NiMo/Al_2O_3$ has the highest MoS_2 dispersion among the oxide supported catalysts. The MoS_2 dispersion of $NiMo/SiO_2$ and NiMo/ASA is only slightly lower. The average stacking degree increases with decreasing metal-support interaction (alumina > ASA > SiO_2). Compared with these oxide-supported catalysts, the MoS_2 dispersion on activated carbon is considerably higher. At the same time, the stacking degree of the MoS_2 phase is higher for NiMo/C than for the other catalysts. The high MoS_2 dispersion of NiMo/C is due to the very high surface area of the activated carbon, even though the Mo-precursor will likely only weakly interact with the activated carbon support. It has been discussed before that the carbon support stabilizes very small MoS_2 slabs and that the active phase should have a pronounced type II character [55]. The MoS_2 dispersion, *i.e.* the fraction of Mo atoms at the edges of the MoS_2 slabs, was determined from the average slab length, using the geometrical model of Kasztelan et al. based on perfect hexagons [50]. The resulting values for the edge dispersion are given in Table 2.

X-ray photoelectron spectroscopy (XPS) was used to determine differences in the extent of sulfidation of the freshly sulfided catalysts (Fig. 3). The Ni $2p_{3/2}$ spectrum contains contributions of Ni^{2+} in sulfidic and oxidic environment. Shake-up features related to these species are seen at higher binding energies [56]. The Mo 3d spectrum is mainly composed of MoS_2 (Mo^{4+}) with small contributions of Mo-oxysulfides (Mo^{5+}) and $-$oxides (Mo^{6+}). The Mo 3d spectra were
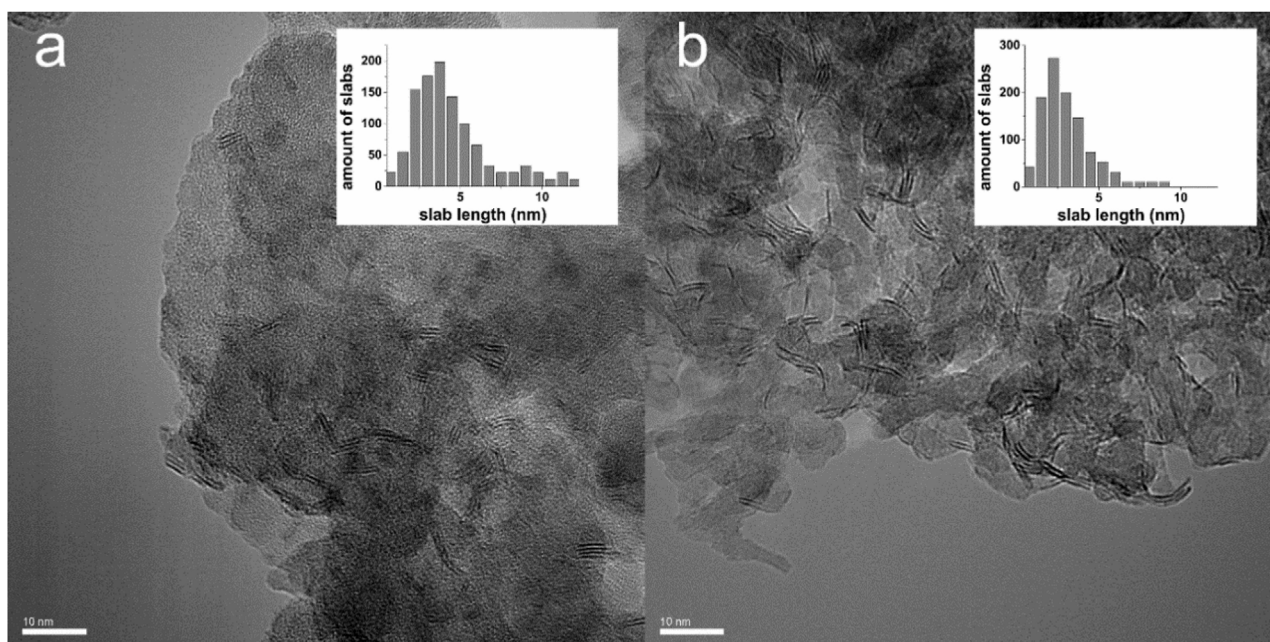
Fig. 2. Representative TEM micrographs of sulfided (a) NiMo/SiO$_2$ and (b) NiMo/Al$_2$O$_3$ (catalysts were sulfided at 15 bar in a 10 vol% H$_2$S in H$_2$ flow whilst heating at a rate of 2 °C/min to 400 °C with a dwell of 2 h). The inserts show the slab length distribution.

fitted with three doublets, representing these Mo^{4+}, Mo^{5+}, and Mo^{6+} contributions [57], and a feature due to S 2s. The fits of the Ni 2p$^{3/2}$ and Mo 3d spectra are shown in Fig. 3. Quantitative data are collected in Table 2. The sulfidation degree, as indicated by the contribution of Mo^{4+}, does not vary significantly among the different catalysts and amounts to 80–90%. There is no systematic trend in the contribution of Mo^{5+} and Mo^{6+} between the various catalysts.

To gauge performance differences of the sulfided catalysts, gas phase thiophene HDS was performed. The overall reaction rates on a per mol Mo basis are collected in Table 2. As expected, the sulfided NiMo/C catalyst displays much higher HDS activity than the oxide-supported NiMo sulfides [35]. The difference is much larger than can be expected based on the dispersion differences. Among the oxide-supported catalysts, NiMo/Al$_2$O$_3$ and NiMo/SiO$_2$ show comparable HDS activities, whilst the NiMo/ASA sample is less active. A reference NiMo/Al$_2$O$_3$ catalyst prepared without NTA had a lower activity (34 mol mol^{-1} h^{-1}) than the NTA-prepared NiMo/Al$_2$O$_3$, consistent with the notion that the use of NTA increases the type II character and, accordingly, the thiophene HDS activity. The reason for the lower activity of the NiMo/ASA catalyst is not clear. We speculate that the strong Lewis acidic Al^{3+} sites present in larger amounts on amorphous

silica-alumina than on alumina might act as strong anchoring points for the Mo-oxide precursors, even when NTA is used in the preparation. This would mean that the active phase in NiMo/ASA has a less pronounced type II character than in NiMo/Al$_2$O$_3$.

All sulfided samples were evaluated for their catalytic performance in the HDO of methyl oleate. Methyl oleate HDO was carried out at a temperature of 260 °C and a total pressure of 30 bar. The reaction time was 1 week in order to follow catalyst deactivation. The main HDO reaction products observed during methyl oleate HDO were octadecane, octadecenes, heptadecane and heptadecenes. As reported earlier for sulfided NiMo/Al$_2$O$_3$ [44], a large part of the methyl oleate reactant is hydrogenated to methyl stearate (octadecanoic methyl ester). In addition, stearic (octadecanoic) acid and oleic (octadecenoic) acid were among the reaction products. Alcohols and aldehydes were not observed by online GC analysis nor by GC analysis of the condensed reactor effluent. From the small amounts of stearyl stearate (octadecyl octadecanoate) detected, we infer that octadecanol is a reaction intermediate. The Brønsted acidity of zeolites can cause hydrocracking reactions of alkanes under typical HDS [43] and HDO [58] reaction conditions. This may also happen with acidic amorphous silica-alumina [37]. However, we did not observe cracking of the primary C17 and

Table 2
HR-TEM analysis, XPS and thiophene HDS reaction experiments.

sample	TEM results			atomic ratios from XPS[d]						Thiophene HDS rate[f] (mol/mol/h)
	slab length[a] (nm)	stacking[b] (−)	fMo[c] (−)	Mo^{4+} (%)[e]	Mo^{5+} (%)	Mo^{6+} (%)	B.E. Mo^{4+} (eV)	NiS (%)	Ni/Mo (−)	
NiMo/C	2.1	2.3	0.50	82	11	7.3	228.7	70	0.25	101
NiMo/SiO$_2$	3.3	2.0	0.35	77	17	6.0	229.4	72	0.33	47
NiMo/ASA	3.2	1.7	0.36	87	5.8	7.2	229.3	76	0.28	28
NiMo/Al$_2$O$_3$	2.8	1.4	0.40	90	0.6	10	229.1	76	0.29	38

[a] Determined by fitting a log-normal distribution, 95% confidence norm is 0.1 nm.
[b] 95% confidence norm is 0.1 (−).
[c] Mo edge dispersion as determined by the geometrical model of Kasztelan et al. [49].
[d] Calculated after correcting intensity with relative sensitivity factors based on Scofield cross-sections.
[e] Used as the sulfidation degree.
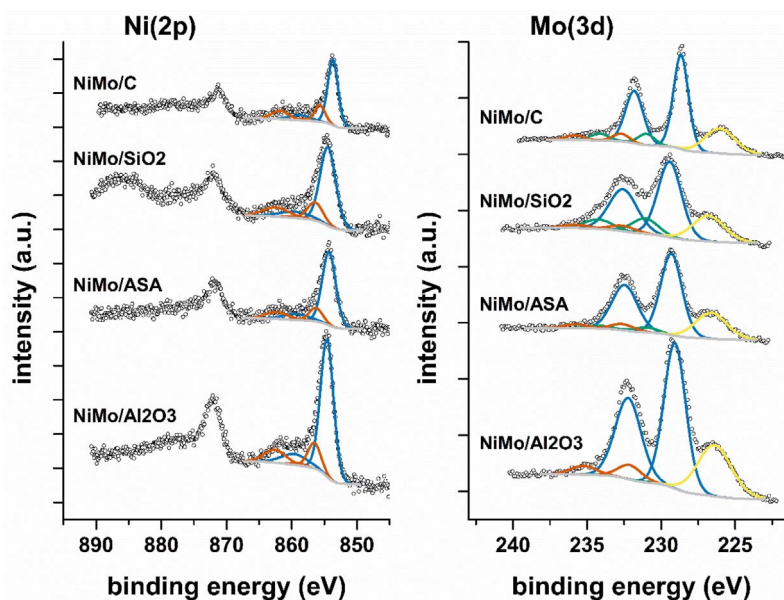[f] Gas phase thiophene HDS at 350 °C and 1 bar corrected for Mo edge dispersion.

Fig. 3. XPS spectra and fits for sulfided NiMo/C, NiMo/SiO$_2$, NiMo/ASA and NiMo/Al$_2$O$_3$. Fits for sulfided species in blue and (sulfur)oxide species in red. The contribution for sulfur in the Mo(3d) spectra is indicated in yellow. All catalysts were sulfided in 15 bar 10 vol% H$_2$S in H$_2$ whilst heating at a rate of 2 °C/min to 400 °C with a dwell of 2 h. (For interpretation of the references to colour in this figure legend, the reader is referred to the web version of this article.)
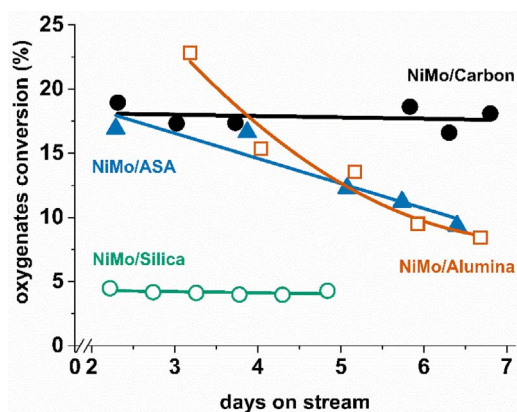

Fig. 4. Conversion of oxygenated ccompounds using (●) NiMo/C, (○) NiMo/SiO$_2$, (▲) NiMo/ASA, and (□) NiMo/Al$_2$O$_3$. The lines are meant to guide the eye. Reactions were performed at 260 °C and a pressure of 30 bar using methyl oleate as the feedstock in hydrogen at a gas-to-oil ratio of 10,320 Nl kg^{-1} h^{-1}. The feed contained 2000 ppm H$_2$S.

C18 reaction products obtained by methyl oleate HDO, which is most likely due to the relatively low reaction temperature.

Fig. 4 shows the conversion for the overall deoxygenation for methyl oleate as a function of time on stream. These data already evidence the substantial differences in initial activity and deactivation. As the catalysts exhibit different MoS$_2$ dispersion, we further discuss their activities in terms of edge-atom-normalized values.

Fig. 5a shows the dispersion-corrected pseudo first-order rate constant for the overall HDO reaction of methyl oleate to hydrocarbons as a function of time on stream for the different catalysts. Considerable differences in the overall HDO activity and rate of deactivation are observed. Whereas NiMo/C and NiMo/SiO$_2$ display stable HDO activity, NiMo/Al$_2$O$_3$ and NiMo/ASA deactivate. Initially, NiMo/Al$_2$O$_3$ and NiMo/ASA show higher activity than NiMo/C. After one week on stream, NiMo/C is the most active catalyst. The much higher activity of Ni-promoted MoS$_2$ on activated carbon than on silica points to a strong support effect, in line with findings for thiophene HDS [35]. Fig. 5b highlights that the support also has a strongly effect on the HDO selectivity. The C18 selectivities for NiMo/Al$_2$O$_3$ and NiMo/ASA are much lower than for NiMo/SiO$_2$ and NiMo/C. High C18 selectivity is

desirable, because CO by-product obtained in C17 formation by decarbonylation consumes hydrogen in its conversion to methane.

The first step in the conversion of methyl oleate is hydrolysis of the ester bond. This step is relatively slow and can be catalyzed by Lewis acid surface sites [25,44]. Accordingly, we can relate the higher initial activity of NiMo/Al$_2$O$_3$ and NiMo/ASA compared with NiMo/SiO$_2$ and NiMo/C to the presence of Al^{3+} sites on the Al-containing support surfaces. Although the ASA support contains less LAS, they are stronger than the greater number of LAS on Al$_2$O$_3$. As shown before [44], deposition of heavy products on the support blocks these Al^{3+} sites and slows the rate of methyl ester hydrolysis. This provides a reasonable explanation for the deactivation of NiMo/Al$_2$O$_3$ and NiMo/ASA. We speculate that the active metal sulfide phase is also involved in hydrolysis of methyl oleate, although at a much lower rate.

Oleic acid is the product of methyl oleate hydrolysis [25,31] and can be hydrogenated to stearic acid. The amount of these intermediate acids was relatively low for all. Stearyl stearate is the product of the esterification of oleic acid with intermediate alcohols. Only (fully hydrogenated) stearyl stearate is observed in the HDO experiments, which is likely due to the long residence time of the heavy esters in the reactor.

We observed that the stearyl stearate yield decreased for NiMo/Al$_2$O$_3$ and NiMo/ASA with time on stream, but remained constant for NiMo/C and NiMo/SiO$_2$ (Fig. 6). This difference can be explained in the following manner. The decreased hydrolysis rate due to catalyst deactivation results in lower concentration of intermediate acids and, consequently, lower yield of stearyl stearate. It is also seen that at the time scale of the HDO measurements the stearyl stearate yields of NiMo/Al$_2$O$_3$ and NiMo/ASA approach that of NiMo/SiO$_2$. The corresponding yield for stearyl stearate of NiMo/C is much higher and constant. Relatively speaking, the rate of HDO conversion of the intermediate acids to hydrocarbons is less affected by the deactivation than the initial hydrolysis step. The higher yield for NiMo/C also shows that this catalyst is relatively more active in methyl oleate hydrolysis than NiMo/SiO$_2$. On the one hand, this might be an intrinsic property of the active metal sulfide phase on carbon, which would be consistent with higher intrinsic activity in HDS reactions. On the other hand, we cannot rule out that acid sites such as carboxylic groups on the activated carbon surface may also contribute to the high rate of methyl oleate hydrolysis.
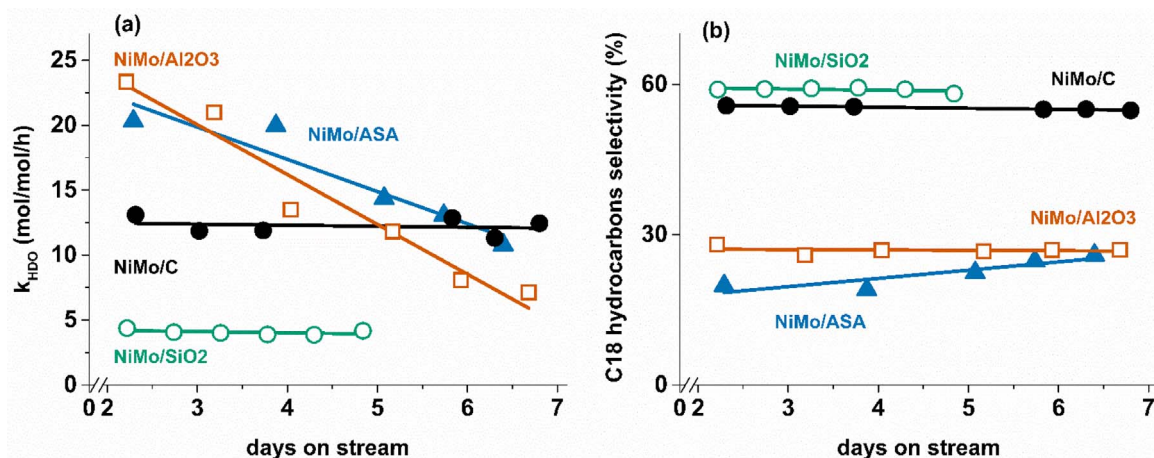
Fig. 5. First-order HDO reaction rate constant (a) and (b) selectivity towards C18 for sulfided (●) NiMo/C, (○) NiMo/SiO$_2$, (▲) NiMo/ASA, and (□) NiMo/Al$_2$O$_3$. The lines are meant to guide the eye. Reactions were performed at 260 °C and a pressure of 30 bar using methyl oleate as the feedstock in hydrogen at a gas-to-oil ratio of 10,320 Nl kg^{-1} h^{-1}. The feed contained 2000 ppm H$_2$S.
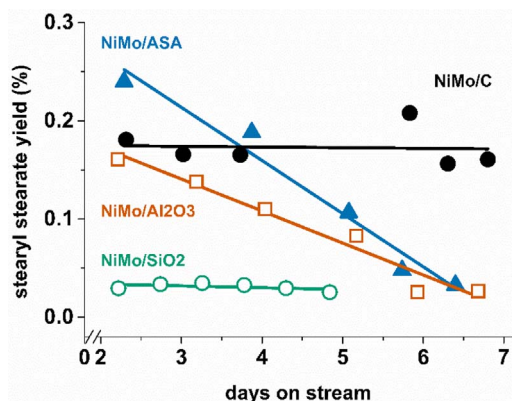

Fig. 6. Yield of stearyl stearate upon time on stream. Shown are sulfided (●) NiMo/C, (○) NiMo/SiO$_2$, (▲) NiMo/ASA, and (□) NiMo/Al$_2$O$_3$. The lines are meant to guide the eyes. Reactions were performed at 260 °C, 30 bar, using methyl oleate as a feedstock and GOR of 10,320 Nl kg^{-1} h^{-1}. 2000 ppm H$_2$S was co-fed.

Based on our previous work and the extensive knowledge in the field of hydrotreating with Ni- and Co-promoted MoS$_2$ catalysts, the active metal sulfide phase in sulfided NiMo contains different sites for hydrogenolysis and hydrogenation [18,44]. The active phase is likely also involved in hydrolysis reactions of the methyl ester, presumably through slightly acidic SH groups adsorbed on the metal sulfide. The Al-containing catalysts (NiMo/ASA and NiMo/Al$_2$O$_3$) also contain Lewis acidic sites on the support surface, which contribute to methyl ester hydrolysis but also to side-reactions that lead to deposition of heavy products on the surface. Weak Brønsted acid sites, presumably carboxylic groups, on the carbon support may also be involved in methyl ester hydrolysis. The activity data thus confirm that the activity in methyl oleate HDO is mainly determined by the rate of methyl ester hydrolysis. Deactivation of the Lewis acid sites in Al-containing supports results in a strong decrease of the overall HDO activity. This deactivation does not occur with NiMo/SiO$_2$ and NiMo/C. A significant difference is the much lower C18 hydrocarbons selectivity for NiMo/Al$_2$O$_3$ and NiMo/ASA as compared with NiMo/SiO$_2$ and NiMo/C. These observations combined also imply that the presence of Brønsted acidic sites (BAS) [45] has no influence on the HDO perfomance. The low C18 hydrocarbons selectivity of NiMo/Al$_2$O$_3$ is consistent with earlier work employing a commercial γ-Al$_2$O$_3$ supported NiMo sulfide catalyst [44]. This difference points to a difference in the rate of hydrogenation of the fatty aldehyde to the fatty alcohol. It has been demonstrated that this reaction is more complex than a simple hydrogenation of the aldehyde,

instead involving a keto-enol equilibrium [31]. Thus, we speculate that the differences observed here is a support effect, likely caused by the type I/II character of the active phase.

4. Conclusions

The influence of the support on the hydrodeoxygenation of methyl oleate by sulfided NiMo was evaluated in a trickle flow reactor. The support materials investigated were activated carbon, silica, γ-alumina and ASA. The active phase was loaded by incipient wetness impregnation in the presence of NTA. Sulfidation resulted in nearly similar sulfidation degree (80–90%) for all catalysts. The MoS$_2$ dispersion increased in the order NiMo/SiO$_2$ < NiMo/ASA < NiMo/Al$_2$O$_3$ < NiMo/C. The stacking degree showed a different trend namely NiMo/Al$_2$O$_3$ < NiMo/ASA < NiMo/SiO$_2$ < NiMo/C. Despite the use of NTA as chelating agent to suppress metal-support interactions, the support had a significant influence on the morphology of the active phase. A support effect was also noted for the dispersion-corrected activity in thiophene HDS. NiMo/C was twice as active as NiMo/SiO$_2$. NiMo/Al$_2$O$_3$ and NiMo/ASA had lower thiophene HDS activities than NiMo/SiO$_2$. In methyl oleate HDO, all catalysts could convert the model compound for triglyciderides to C17 and C18 olefins and paraffins. Whilst initially NiMo/Al$_2$O$_3$ and NiMo/ASA displayed the highest overall HDO activity, these catalysts deactivated during the week on stream. At the end of the run, they had similar activity as NiMo/SiO$_2$. On the other hand, NiMo/C and NiMo/SiO$_2$ did not deactivate. The NiMo/C catalyst was appreciably more active than the others after prolonged reaction. The high initial and then deactivating performance of NiMo/Al$_2$O$_3$ and NiMo/ASA is linked to the Lewis acidity of surface Al species active in methyl oleate hydrolysis. It has earlier been demonstrated that deposition of heavy products on the alumina surface deactivates these sites. SiO$_2$ lacks such sites, resulting in lower catalytic performance. The presence of BAS (in ASA) has no influence on the process under these conditions. The NiMo/C support is more active in methyl oleate hydrolysis. This can be either due to an intrinsically higher activity of the active metal sulfide phase in this reaction or to acidic surface groups. Besides, the reaction data show that the C18 hydrocarbons selectivity for NiMo/SiO$_2$ and NiMo/C is substantially higher than for the other two catalysts. Clearly, the support has a significant influence on the performance of NiMo sulfide in methyl oleate HDO. The use of activated carbon as the support presents high and stable HDO activity of methyl oleate with good C18 hydrocarbons selectivity. This study suggests the promise of activated carbon as a support for NiMo sulfide catalyzed HDO of vegetable oils, fats and greases into clean diesel.

Acknowledgement

References

[1] Energyroadmap 2050, Brussel, 2011. http://eur-lex.europa.eu/legal-content/EN/TXT/PDF/?uri=CELEX:52011DC0885&from=NL.

[2] International Energy Agency, Medium-Term Market Report 2015-Market Analysis and Forecasts to 2020, (2015), pp. 1–140, http://www.iea.org/publications/freepublications/publication/MTOMR_2015_Final.pdf.

[3] European Commission, Innovating for sustainable growth: a bioeconomy for Europe, Ind. Biotechnol. 8 (2012) 57–61, http://dx.doi.org/10.1089/ind.2012.1508.

[4] I. Kubičková, D. Kubička, Utilization of triglycerides and related feedstocks for production of clean hydrocarbon fuels and petrochemicals: a review, Waste Biomass Valorization 1 (2010) 293–308, http://dx.doi.org/10.1007/s12649-010-9032-8.

[5] M. Grilc, B. Likozar, J. Levec, Hydrodeoxygenation and hydrocracking of solvolysed lignocellulosic biomass by oxide, reduced and sulphide form of NiMo, Ni, Mo and Pd catalysts, Appl. Catal. B Environ. 150–151 (2014) 275–287, http://dx.doi.org/10.1016/j.apcatb.2013.12.030.

[6] M. Grilc, B. Likozar, J. Levec, Simultaneous liquefaction and hydrodeoxygenation of lignocellulosic biomass over NiMo/Al 2O3, Pd/Al2O3, and zeolite Y catalysts in hydrogen donor solvents, ChemCatChem 8 (2016) 180–191, http://dx.doi.org/10.1002/cctc.201500840.

[7] R.W. Gosselink, S.A.W. Hollak, S.-W. Chang, J. van Haveren, K.P. de Jong, J.H. Bitter, D.S. van Es, Reaction pathways for the deoxygenation of vegetable oils and related model compounds, ChemSusChem 6 (2013) 1576–1594, http://dx.doi.org/10.1002/cssc.201300370.

[8] T.V. Choudhary, C.B. Phillips, Renewable fuels via catalytic hydrodeoxygenation, Appl. Catal. A Gen. 397 (2011) 1–12, http://dx.doi.org/10.1016/j.apcata.2011.02.025.

[9] S. Lestari, P. Mäki-Arvela, J. Beltramini, G.Q.M. Lu, D.Y. Murzin, Transforming triglycerides and fatty acids into biofuels, ChemSusChem 2 (2009) 1109–1119, http://dx.doi.org/10.1002/cssc.200900107.

[10] I. Kubičková, M. Snåre, K. Eränen, P. Mäki-Arvela, D.Y. Murzin, Hydrocarbons for diesel fuel via decarboxylation of vegetable oils, Catal. Today 106 (2005) 197–200, http://dx.doi.org/10.1016/j.cattod.2005.07.188.

[11] W. Charusiri, T. Vitidsant, Kinetic study of used vegetable oil to liquid fuels over sulfated zirconia, Energy Fuels 19 (2005) 1783–1789, http://dx.doi.org/10.1021/ef0500181.

[12] R. Tiwari, B.S. Rana, R. Kumar, D. Verma, R. Kumar, R.K. Joshi, M.O. Garg, A.K. Sinha, Hydrotreating and hydrocracking catalysts for processing of waste soya-oil and refinery-oil mixtures, Catal. Commun. 12 (2011) 559–562, http://dx.doi.org/10.1016/j.catcom.2010.12.008.

[13] Honeywell Green Diesel™, (n.d.). http://www.uop.com/processing-solutions/renewables/green-diesel/. (Accessed 4 June 2016).

[14] Production Operation Neste, 2016 https://www.neste.com/en/corporate-info/who-we-are/production. (Accessed 1 January 2016).

[15] Y. Liu, R. Sotelo-Boyás, K. Murata, T. Minowa, K. Sakanishi, Hydrotreatment of vegetable oils to produce bio-Hydrogenated diesel and liquefied petroleum gas fuel over catalysts containing sulfided Ni-Mo and solid acids, Energy Fuels 25 (2011) 4675–4685, http://dx.doi.org/10.1021/ef200889e.

[16] P. Šimáček, D. Kubička, G. Šebor, M. Pospíšil, Hydroprocessed rapeseed oil as a source of hydrocarbon-based biodiesel, Fuel 88 (2009) 456–460, http://dx.doi.org/10.1016/j.fuel.2008.10.022.

[17] R. Sotelo-Boyás, Y. Liu, T. Minowa, Renewable diesel production from the hydrotreating of rapeseed oil with Pt/zeolite and NiMo/Al2O3 catalysts, Ind. Eng. Chem. Res. 50 (2011) 2791–2799, http://dx.doi.org/10.1021/ie100824d.

[18] H. Topsøe, B.S. Clausen, F.E. Massoth, Hydrotreating Catalysis Science and Technology, Springer-Verlag, New York, 1996.

[19] R. Prins, V.H.J. de Beer, G.A. Somorjai, Structure and function of the catalyst and the promoter in Co–Mo hydrodesulfurization catalysts, Catal. Rev. 31 (1989) 1–41, http://dx.doi.org/10.1080/01614949089351347.

[20] P.T. Vasudevan, J.L. García Fierro, A review of deep hydrodesulfurization catalysis, Catal. Rev. 38 (1996) 161–188, http://dx.doi.org/10.1080/01614949608006457.

[21] S. Eijsbouts, On the flexibility of the active phase in hydrotreating catalysts, Appl. Catal. A Gen. 158 (1997) 53–92. http://www.sciencedirect.com/science/article/pii/S0926860X97000355 . (Accessed 13 December 2012).

[22] M. Breysse, E. Furimsky, S. Kasztelan, M. Lacroix, G. Perot, Hydrogen activation by transition metal sulfides, Catal. Rev. 44 (2002) 651–735, http://dx.doi.org/10.1081/CR-120015483.

[23] E. Furimsky, Hydroprocessing challenges in biofuels production, Catal. Today 217 (2013) 13–56, http://dx.doi.org/10.1016/j.cattod.2012.11.008.

[24] E. Laurent, B. Delmon, Influence of water in the deactivation of a sulfided NiMo/g-Al2O3 catalyst during hydrodeoxygenation, J. Catal. 146 (1994) 281–291. http://www.sciencedirect.com/science/article/pii/0021951794900329 . (Accessed 13 December 2012).

[25] O. Şenol, E.-M. Ryymin, T.-R. Viljava, A.O.I. Krause, Reactions of methyl heptanoate hydrodeoxygenation on sulphided catalysts, J. Mol. Catal. A Chem. 268 (2007) 1–8, http://dx.doi.org/10.1016/j.molcata.2006.12.006.

[26] O. Şenol, T.-R. Viljava, A.O.I. Krause, Hydrodeoxygenation of aliphatic esters on sulphided NiMo/γ-Al2O3 and CoMo/γ-Al2O3 catalyst: the effect of water, Catal. Today 106 (2005) 186–189, http://dx.doi.org/10.1016/j.cattod.2005.07.129.

[27] O. Şenol, T.-R. Viljava, A.O.I. Krause, Effect of sulphiding agents on the hydro-deoxygenation of aliphatic esters on sulphided catalysts, Appl. Catal. A Gen. 326 (2007) 236–244, http://dx.doi.org/10.1016/j.apcata.2007.04.022.

[28] O. Şenol, T.-R. Viljava, A.O.I. Krause, Hydrodeoxygenation of methyl esters on sulphided NiMo/γ-Al2O3 and CoMo/γ-Al2O3 catalysts, Catal. Today 100 (2005) 331–335, http://dx.doi.org/10.1016/j.cattod.2004.10.021.

[29] D. Kubička, M. Bejblová, J. Vlk, Conversion of vegetable oils into hydrocarbons over CoMo/MCM-41 catalysts, Top. Catal. 53 (2010) 168–178, http://dx.doi.org/10.1007/s11244-009-9421-z.

[30] C. Dupont, R. Lemeur, A. Daudin, P. Raybaud, Hydrodeoxygenation pathways catalyzed by MoS2 and NiMoS active phases: a DFT study, J. Catal. 279 (2011) 276–286, http://dx.doi.org/10.1016/j.jcat.2011.01.025.

[31] B. Donnis, R.G. Egeberg, P. Blom, K.G. Knudsen, Hydroprocessing of bio-oils and oxygenates to hydrocarbons. Understanding the reaction routes, Top. Catal. 52 (2009) 229–240, http://dx.doi.org/10.1007/s11244-008-9159-z.

[32] D. Kubička, J. Horáček, Deactivation of HDS catalysts in deoxygenation of vegetable oils, Appl. Catal. A Gen. 394 (2011) 9–17, http://dx.doi.org/10.1016/j.apcata.2010.10.034.

[33] O. Şenol, E.-M. Ryymin, T.-R. Viljava, A.O.I. Krause, Effect of hydrogen sulphide on the hydrodeoxygenation of aromatic and aliphatic oxygenates on sulphided catalysts, J. Mol. Catal. A Chem. 277 (2007) 107–112, http://dx.doi.org/10.1016/j.molcata.2007.07.033.

[34] E.-M. Ryymin, M.L. Honkela, T.-R. Viljava, A.O.I. Krause, Insight to sulfur species in the hydrodeoxygenation of aliphatic esters over sulfided NiMo/γ-Al2O3 catalyst, Appl. Catal. A Gen. 358 (2009) 42–48, http://dx.doi.org/10.1016/j.apcata.2009.01.035.

[35] J.A.R. van Veen, E. Gerkema, A.M. van der Kraan, A. Knoester, A real support effect on the activity of fully sulphided CoMoS for the hydrodesulphurization of thiophene, J. Chem. Soc. Chem. Commun. (1987) 1684–1686. http://pubs.rsc.org/en/content/articlepdf/1987/c3/c39870001684 . (Accessed 13 December 2012).

[36] L. Medici, R. Prins, The influence of chelating ligands on the sulfidation of Ni and Mo in NiMo/SiO2 hydrotreating catalysts, J. Catal. 163 (1996) 38–49 (isi:A1996VL08800005).

[37] A.E. Coumans, D.G. Poduval, J.A.R. van Veen, E.J.M. Hensen, The nature of the sulfur tolerance of amorphous silica-alumina supported NiMo(W) sulfide and Pt hydrogenation catalysts, Appl. Catal. A Gen. 411–412 (2012) 51–59, http://dx.doi.org/10.1016/j.apcata.2011.10.022.

[38] H. Topsøe, B.S. Clausen, Active sites and support effects in hydrodesulfurization catalysts, Appl. Catal. 25 (1986) 273–293, http://dx.doi.org/10.1016/S0166-9834(00)81246-4.

[39] A.I. Dugulan, J.A.R. van Veen, E.J.M. Hensen, On the structure and hydrotreating performance of carbon-supported CoMo- and NiMo-sulfides, Appl. Catal. B Environ. 142–143 (2013) 178–186, http://dx.doi.org/10.1016/j.apcatb.2013.05.013.

[40] T. Morgan, D. Grubb, E. Santillan-Jimenez, M. Crocker, Conversion of triglycerides to hydrocarbons over supported metal catalysts, Top. Catal. 53 (2010) 820–829, http://dx.doi.org/10.1007/s11244-010-9456-1.

[41] S. Harnos, G. Onyestyák, D. Kalló, Hydrocarbons from sunflower oil over partly reduced catalysts, React. Kinet. Mech. Catal. 106 (2012) 99–111, http://dx.doi.org/10.1007/s11144-012-0424-6.

[42] E. Santillan-Jimenez, T. Morgan, J. Lacny, S. Mohapatra, M. Crocker, Catalytic deoxygenation of triglycerides and fatty acids to hydrocarbons over carbon-supported nickel, Fuel 103 (2013) 1010–1017, http://dx.doi.org/10.1016/j.fuel.2012.08.035.

[43] G. Busca, Acid catalysts in industrial hydrocarbon chemistry, Chem. Rev. 107 (2007) 5366–5410, http://dx.doi.org/10.1021/cr068042e.

[44] A.E. Coumans, E.J.M. Hensen, A model compound (methyl oleate, oleic acid, triolein) study of triglycerides hydrodeoxygenation over an alumina-supported NiMo sulfide, Catal. Appl. Catal. B Environ. (2017), http://dx.doi.org/10.1016/j.apcatb.2016.08.036.

[45] E.J.M. Hensen, D.G. Poduval, P.C.M.M. Magusin, A.E. Coumans, J.A.R. van Veen, Formation of acid sites in amorphous silica-alumina, J. Catal. 269 (2010) 201–218, http://dx.doi.org/10.1016/j.jcat.2009.11.008.

[46] E.J.M. Hensen, D. Poduval, V. Degirmenci, D.A.J.M. Ligthart, W. Chen, F. Maugé, M.S. Rigutto, J.A.R. van Veen, Acidity characterization of amorphous silica-alumina, J. Phys. Chem. C. 116 (2012) 21416–21429, http://dx.doi.org/10.1021/jp309182f.

[47] P.J. Kooyman, J.A.R. van Veen, The detrimental effect of exposure to air on supported MoS2, Catal. Today 130 (2008) 135–138, http://dx.doi.org/10.1016/j.cattod.2007.07.019.

[48] M.H. Al-Dahhan, F. Larachi, M.P. Dudukovic, A. Laurent, High-pressure trickle-bed reactors: a review, Ind. Eng. Chem. Res. 36 (1997) 3292–3314, http://dx.doi.org/10.1021/ie9700829.

[49] G.F. Froment, K.B. Bischoff, Chemical Reactor Analysis and Design, 2nd ed., John Wiley & Sons, Inc, Singapore, 1990.

[50] S. Kasztelan, H. Toulhoat, J. Grimblot, J.P. Bonnelle, A geometrical model of the active phase of hydrotreating catalysts, Appl. Catal. 13 (1984) 127–159, http://dx.doi.org/10.1016/S0166-9834(00)83333-3.

[51] M.-H. Lee, C.-F. Cheng, V. Heine, J. Klinowski, Distribution of tetrahedral and octahedral A1 sites in gamma alumina, Chem. Phys. Lett. 265 (1997) 673–676, http://dx.doi.org/10.1016/S0009-2614(96)01492-3.

[52] M.F. Williams, B. Fonfe, C. Sievers, A. Abraham, J.A. van Bokhoven, A. Jentys, J.A.R. van Veen, J.A. Lercher, Hydrogenation of tetralin on silica-alumina-supported Pt catalysts I. Physicochemical characterization of the catalytic materials, J. Catal. 251 (2007) 485–496, http://dx.doi.org/10.1016/j.jcat.2007.06.009.

[53] E.J.M. Hensen, Y. van der Meer, J.A.R. van Veen, J.W. Niemantsverdriet, Insight

into the formation of the active phases in supported NiW hydrotreating catalysts, Appl. Catal. A Gen. 322 (2007) 16–32, http://dx.doi.org/10.1016/j.apcata.2007.01.003.

[54] E.J.M. Hensen, P.J. Kooyman, Y. van der Meer, A.M. van der Kraan, V.H.J. de Beer, J.A.R. van Veen, R.A. van Santen, The relation between morphology and hydro-treating activity for supported MoS2 particles, J. Catal. 199 (2001) 224–235, http://dx.doi.org/10.1006/jcat.2000.3158.

[55] E.J.M. Hensen, V.H.J. de Beer, J.A.R. van Veen, R.A. van Santen, On the sulfur tolerance of supported Ni(Co)Mo sulfide hydrotreating catalysts, J. Catal. 215 (2003) 353–357, http://dx.doi.org/10.1016/S0021-9517(03)00012-5.

[56] Kung T. Ng, D.M. Hercules, Studies of nickel-tungsten-alumina catalysts by X-ray photoelectron spectroscopy, J. Phys. Chem. 80 (1976) 2094–2102, http://dx.doi.org/10.1021/j100560a009.

[57] T.A. Patterson, J.C. Carver, D.E. Leyden, D.M. Hercules, A surface study of cobalt-molybdena-alumina catalysts using x-ray photoelectron spectroscopy, J. Phys. Chem. 80 (1976) 1700–1708, http://dx.doi.org/10.1021/j100556a011.

[58] H. Zuo, Q. Liu, T. Wang, L. Ma, Q. Zhang, Q. Zhang, Hydrodeoxygenation of methyl palmitate over supported Ni catalysts for diesel-like fuel production, Energy Fuels 26 (2012) 3747–3755, http://dx.doi.org/10.1021/ef300063b.